

Simulation of Thermal Surface Waves in a Protoplanetary Disk in a Two-Dimensional Approximation

Ya. N. Pavlyuchenkov, L. A. Maksimova, V. V. Akimkin

Institute of Astronomy RAS, Moscow, Russia

Received 10.06.2022; revised 11.08.2022; accepted 30.08.2022

pavyar@inasan.ru

ABSTRACT

Theoretical models predict that the obscuration of stellar radiation by irregularities on the surface of a protoplanetary disk can cause self-generating waves traveling towards the star. However, this process is traditionally simulated using the 1+1D approach, the key approximations of which — vertical hydrostatic equilibrium of the disk and vertical diffusion of IR radiation — can distort the picture. This article presents a two-dimensional radiative hydrodynamic model of the evolution of an axially symmetric gas and dust disk. Within this model, but using simplified assumptions from 1+1D models, we have reproduced the spontaneous generation and propagation of thermal surface waves. The key conclusion of our work is that taking into account two-dimensional hydrodynamics and diffusion of IR radiation suppresses the spontaneous generation and development of thermal waves observed in the 1+1D approximation. The search for the possibility of the existence of surface thermal waves should be continued by studying the problem for various parameters of protoplanetary disks.

Keywords: physical processes and instabilities in protoplanetary disks, numerical simulation of gas and dust disks of young stars

DOI: 10.1134/S1063772922100110

1 INTRODUCTION

In protoplanetary disks, conditions for the emergence of a wide variety of dynamic instabilities are realized, the development of which can affect both the observed manifestations and the overall evolution of disks (Velikhov 1959; Balbus & Hawley 1991; Youdin & Goodman 2005; Nelson, Gressel & Umurhan 2013; Klahr & Hubbard 2014; Lesur & Latter 2016; Zhuravlev 2022). One of such instabilities is that associated with the obscuration of stellar radiation by the surface inhomogeneities of the disk (Watanabe & Lin 2008). This instability is due to the positive feedback between the angle at which the star's radiation enters the disk's atmosphere and its heating. Many theoretical models show that a small local distortion of the disk surface can provoke the generation of waves traveling towards the central star, see Ueda, Flock & Birnstiel (2021); Wu & Lithwick (2021); Okuzumi, Ueda & Turner (2022). Such thermal waves on the disk surface were predicted both in the inner regions of passive disks, where the characteristic time of establishment of thermal equilibrium is shorter than the dynamic time (Watanabe & Lin 2008), and on the disk periphery in the reverse situation (Dullemond 2000). In our previous work (Pavlyuchenkov, Maksimova & Akimkin 2022), we also reproduced the process of formation of thermal waves and found that they can affect only the upper layers of disks without significant temperature fluctuations in the equatorial plane.

However, the 1+1D approach used by Pavlyuchenkov, Maksimova & Akimkin (2022), as in most other works on this prob-

lem, is based on several key approximations that can significantly distort the real picture. Such approximations are 1) the absence of diffusion of thermal radiation in the radial direction and 2) hydrostatic equilibrium in the vertical direction and the absence of gas-dynamic effects in the radial direction. The gradual abandonment of these assumptions is important for substantiating the reality of thermal waves in real disks.

In particular, in recent paper by Okuzumi, Ueda & Turner (2022), a two-layer disk model was presented, in which two-dimensional (R, z) effects of heating the equatorial layers by IR radiation from surface layers were considered and the development of instability for various parameters of the numerical model was demonstrated. However, considering the diffusion of IR radiation in the radial direction in even more detail can lead to a wide redistribution of thermal energy in the vicinity of the perturbation, which can smooth out the resulting waves.

The initial perturbation can also be reduced or even completely suppressed by dynamic effects. Indeed, increased pressure in the heated layer can be used not only to lift the layer (as in the 1+1D model), but also to push apart neighboring radial layers. A schematic of these processes is shown in Fig. 1.

The aim of this work is to consider the processes of gas dynamics and diffusion of IR radiation in the excitation of surface thermal waves. This study is conducted using a fully two-dimensional radiative hydrodynamic model. Within this model, we

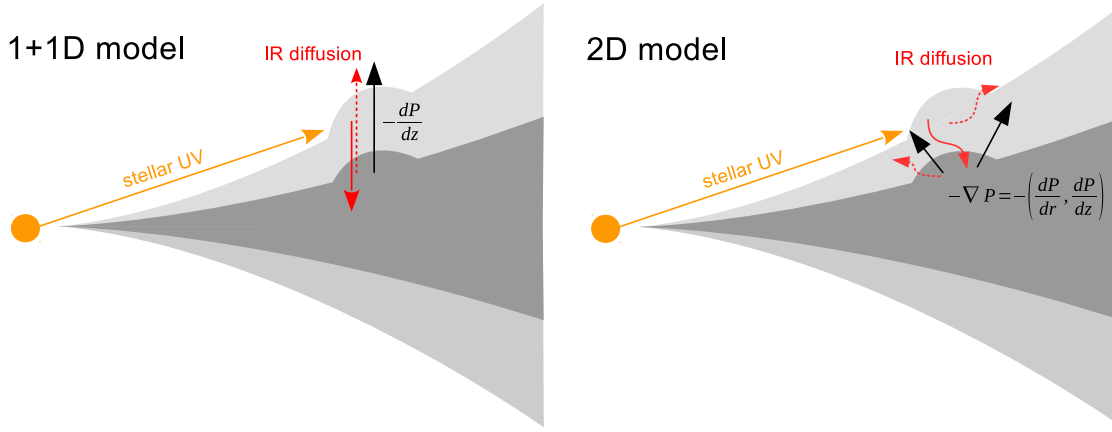


Figure 1. Illustration of the processes during the formation of a hump on the disk surface (left) in the 1+1D model and (right) in the 2D model: (black arrows) the forces associated with the pressure gradient, (red solid arrows) IR radiation that heats the inner layers of the disk, and (red dotted arrows) outgoing IR radiation.

also implemented the simplifying assumptions of the 1+1D approaches in order to determine their validity.

2 BASIC AXISYMMETRIC MODEL OF A PROTOPLANETARY DISK

To simulate the evolution of a gas and dust disk, we use a combination of finite difference methods for hydrodynamics and radiative transfer adapted to a spherical coordinate system. The entire computational domain is divided into cells, within which the values of physical quantities are assumed to be constant. The grid structure is shown in Fig. 2. We consider the spherical coordinate system more convenient than the others, because the calculation of the heating of the medium by the UV radiation of the star (ray tracing in the radial direction) in the spherical coordinates is implemented most easily. Axial symmetry in spherical coordinates is implemented by introducing a single cell in the φ coordinate. In our calculations, we use an inhomogeneous discrete grid refined towards the center in the radial (r) direction and towards the equator when splitting in the angle θ with a resolution of 360 radial \times 64 angular cells. The cell length in the angle φ is taken equal to one degree, which is comparable to the resolution in θ near the equator. Such a grid reflects well the disk structure and makes it possible to trace the resulting gradients of physical quantities. The evolution is calculated using the splitting with respect to physical processes; i.e., the hydrodynamic step is followed by the radiative transfer calculation step.

2.1 Hydrodynamic Method

To describe the dynamic evolution of a gas and dust disk, we use the standard gas dynamics equations for an inviscid gas in divergent form:

$$\frac{\partial \rho}{\partial t} + \nabla \cdot (\rho \mathbf{U}) = 0 \quad (1)$$

$$\frac{\partial}{\partial t} (\rho \mathbf{U}) + \nabla \cdot (\rho \mathbf{U} \mathbf{U} + P) = \rho \mathbf{f} \quad (2)$$

$$\frac{\partial E}{\partial t} + \nabla \cdot (\mathbf{U}(E + P)) = \rho \mathbf{f} \cdot \mathbf{U}, \quad (3)$$

where ρ is the bulk density, \mathbf{U} is the velocity, P is pressure, \mathbf{f} is the gravitational force per unit mass, $E = \frac{P}{\gamma - 1} + \frac{\rho U^2}{2}$ is the total energy of the gas per unit volume, and γ is the adiabatic exponent.

To solve this system, we use the classical Godunov method, a detailed description of which can be found in [Kulikovskiy, Pogorelov & Semenov (2012), Section 3]. In this method, gas-dynamic fluxes through cell boundaries are found as a result of solving the problem of the decay of an arbitrary gas-dynamic discontinuity. In the implementation we use, the discontinuity decay problem is solved exactly using the bisection method for the resulting nonlinear equation. The found fluxes between cells are used to calculate the physical quantities in the cells on a new time layer. The finite-difference scheme was implemented within the formalism described in Abakumov (2014), where Godunov-type difference schemes in curvilinear coordinates, their application in spherical coordinates, and test examples are considered.

Ultimately, the difference scheme we implemented reduces to the following calculations. Let $\mathbf{q} = (\rho, \rho u, \rho v, \rho w, E)^T$ be a vector of conservative variables, where ρ is the bulk density and u , v , and w are the velocity components in the spherical coordinates. To find the value of \mathbf{q}^{n+1} on a new time layer, two steps are performed: the advection step and the step of considering gravitational sources. The advection step is reduced to finding intermediate values \mathbf{q}^* as follows:

$$\mathbf{q}^* = \mathbf{q}^n + \frac{\Delta t}{\Delta V} (\Delta \mathbf{F} + \Delta \mathbf{G} + \Delta \mathbf{H}), \quad (4)$$

where Δt is the time step; ΔV is the volume of the current cell; and $\Delta \mathbf{F}$, $\Delta \mathbf{G}$, and $\Delta \mathbf{H}$ are the fluxes through the corresponding cell faces, the components of which are given in Appendix A. The advection step is followed by the step of taking into account gravity sources, at which the correction for the radial velocity is calculated:

$$u^{n+1} = u^* - \frac{GM}{r^2} \Delta t, \quad (5)$$

where G is the gravitational constant, M is the mass of the central star, and the quantities dependent on it are recalculated, forming the \mathbf{q}^{n+1} values on the new time layer:

$$\mathbf{q}^{n+1} = (\rho^*, \rho^* u^{n+1}, \rho^* v^*, \rho^* w^*, E(u^{n+1}, v^*, w^*))^T. \quad (6)$$

The hydrodynamic method implemented was thoroughly tested. In particular, the numerical solution of the discontinuity de-

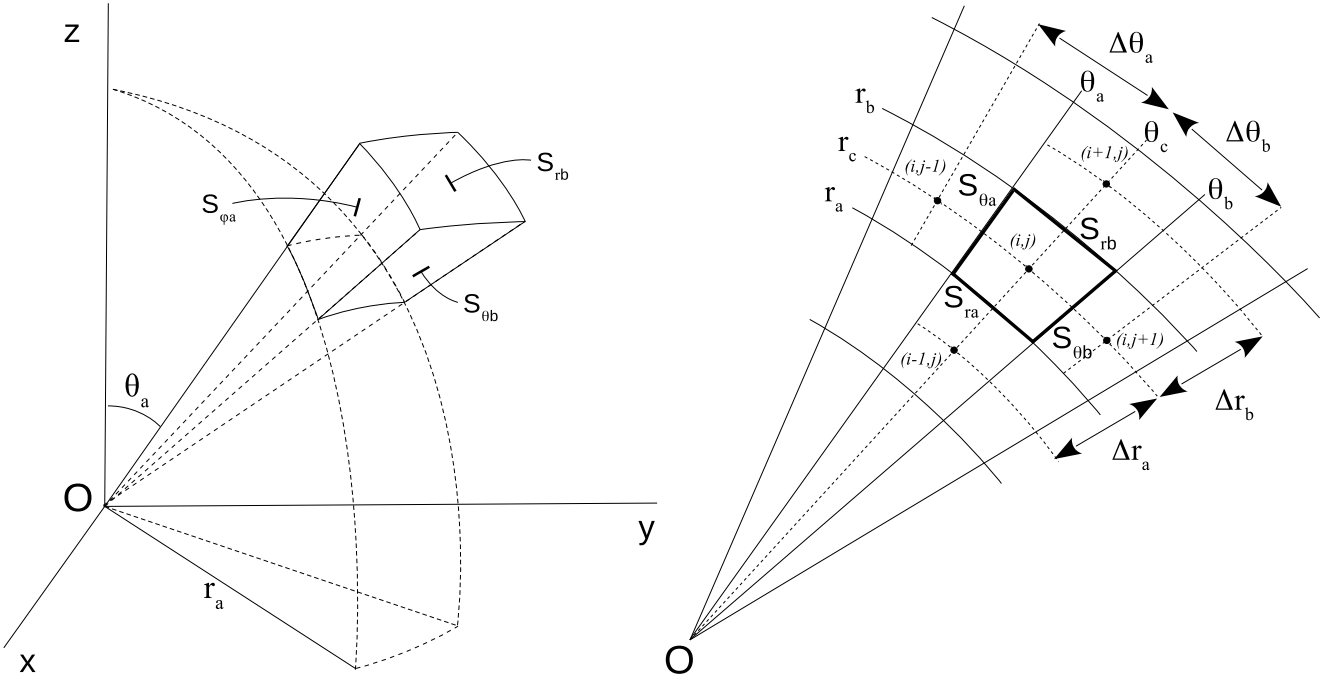


Figure 2. Structure of the computational grid with the designations of quantities: (left) an individual cell in spherical coordinates and (right) polar cut of the grid.

cay problem agrees well with the analytical solution for all types of discontinuities. In addition, we made sure that, within the one-dimensional axisymmetric geometry, the finite-difference approach used gives close results in comparison with the classical approach, in which the source terms associated with the curvilinearity of the coordinate system are clearly distinguished.

2.2 Method for Calculating the Radiative Transfer

To calculate the thermal structure of a gas and dust disk, we use a generalization of the nonstationary thermal model from Vorobyov & Pavlyuchenkov (2017) to the two-dimensional case. The model takes into account the heating of the medium by the direct radiation of the star and diffusion of thermal radiation. The corresponding system of equations has the form

$$\rho c_V \frac{\partial T}{\partial t} = c \rho \kappa_P (E_r - aT^4) + s_* \quad (7)$$

$$\frac{\partial E_r}{\partial t} = -c \rho \kappa_P (E_r - aT^4) + \hat{\Lambda} E_r, \quad (8)$$

where ρ is the density of the gas and dust medium, c_V is the specific heat of the medium [$\text{erg g}^{-1} \text{K}^{-1}$], c is the speed of light, κ_P [$\text{cm}^2 \text{g}^{-1}$] is the Planck-averaged IR radiation true absorption coefficient (without the contribution of scattering, per unit mass of the gas and dust medium), s_* [$\text{erg cm}^{-3} \text{s}^{-1}$] is the rate of heating by stellar radiation, T is the medium temperature, and E_r is the energy density of IR radiation. Equation (7) describes the change in the volumetric thermal energy of the medium as a result of absorption and re-emission of thermal IR radiation (the terms $c \rho \kappa_P E_r$ and $c \rho \kappa_P a T^4$, respectively), as well as a result of absorption of star's direct UV radiation (s_*). Equation (8) is a moment equation of radiative transfer in the Eddington approximation and describes the change in the energy density of IR radiation as a result of absorption and re-emission of thermal IR radiation, as well as a result of

spatial diffusion of IR radiation, represented by the operator $\hat{\Lambda} E_r$:

$$\hat{\Lambda} E_r = -\text{div } \mathbf{F}_r = \text{div} \left(\frac{1}{\sigma} \text{grad } E_r \right), \quad (9)$$

where \mathbf{F}_r is the IR radiation flux, $\sigma = 3 \rho \kappa_R / c$, and κ_R [$\text{cm}^2 \text{g}^{-1}$] is the Rosseland-averaged opacity (taking into account scattering, per unit mass of the gas and dust medium).

Equations (7)–(9) comprise a nonlinear system of diffusion-type partial differential equations. To solve it, we use a completely implicit numerical method, in which the right-hand sides of Eqs. (7)–(8), as well as differential operator (9), depend on the values of the functions on the new time layer:

$$\rho c_V \frac{T - T^n}{\Delta t} = c \rho \kappa_P (E_r - aT^4) + s_* \quad (10)$$

$$\frac{E_r - E_r^n}{\Delta t} = -c \rho \kappa_P (E_r - aT^4) + \hat{\Lambda} E_r, \quad (11)$$

where T^n and E_r^n are the values from the n -th time layer and T and E_r are the sought values on the $(n+1)$ -th time layer for a given spatial cell. In the above equations, for brevity, we suppressed the superscripts of the $(n+1)$ -th time layer of ρ , T , κ_P , s_* and, E_r . We also suppressed the spatial subscripts: for all quantities they correspond to the considered cell (i, j) , except for s_* — the quantity connecting three adjacent cells along the radius, and for the operator connecting the cell (i, j) with four adjacent cells in the radius and the angle θ . The algorithm for solving this system of equations is given in Appendix B.

The UV radiation intensity required for calculating the heating function s_* is found for each cell by direct integration of the equation of radiative transfer from the star to the considered element of the medium in the radial direction. A fundamental point in calculating the function of heating by stellar radiation in our model is considering the radial gradient of the density inside the cell. In our model, the function of volume heating by stellar radiation, s^* [$\text{erg cm}^{-3} \text{s}^{-1}$], is calculated as proposed in Pavlyuchenkov, Mak-

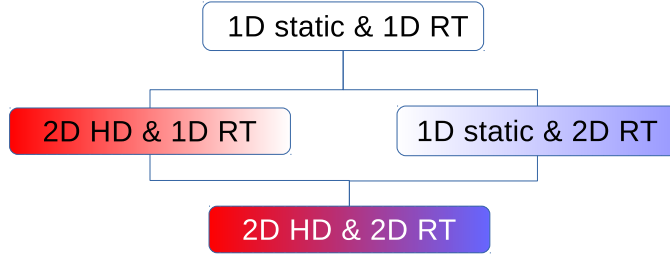


Figure 3. Models of the gas and dust disk under consideration: (static) hydrostatics, (HD) hydrodynamics, and (RT) radiative transfer.

simova & Akimkin (2022):

$$s_* = \rho_m \kappa_{UV} \frac{L \exp(-\tau)}{4\pi r_a^2} \left(\frac{1 - \exp(-\Delta\tau)}{\Delta\tau} \right), \quad (12)$$

where L is the star's luminosity, $\kappa_{UV} = \kappa_p(T_*)$ [$\text{cm}^2 \text{g}^{-1}$] is the stellar radiation absorption coefficient, r_a is the radial distance from the star to the cell's inner boundary, τ is the total optical thickness along the line of sight from the star to the cell's inner boundary, $\Delta\tau = \kappa_p \rho_m \Delta l$ is the optical thickness of the cell itself along the beam, Δl the beam segment length inside the cell, and $\rho_m = \frac{1}{4}(\rho_L + 2\rho_i + \rho_R)$ is the averaged density along the beam. When deriving formula (12) from the formal solution of the radiative transfer equation, it was assumed that the density along the beam inside the cell varies linearly from ρ_L to ρ_i and from ρ_i to ρ_R . The values of ρ_L and ρ_R at the cell boundaries, in turn, are found using a linear interpolation of density between the center of the current cell and the centers of cells adjacent in the radial direction.

The model assumes that the only source of opacity is dust and that the gas and dust temperatures are equal. The ratio between the dust and gas densities throughout the disk is assumed to be constant and equal to 0.01; i.e., dust is assumed to be homogeneously mixed with gas. A specific feature of the thermal model is the use of Planck- and Rosseland-averaged opacities depending on temperature. These coefficients were taken from Pavlyuchenkov et al. (2020), where they are described in detail. Note that we do not use more realistic coefficients that consider, in particular, dust evaporation at high temperatures (see, e.g., Semenov et al. (2003)) in order to limit the number of effects studied.

2.3 Boundary and Initial Conditions

As the initial state, we specify a vertically hydrostatic Keplerian disk with a temperature of 10 K and a distribution of the total ($-\infty < z < \infty$) surface density with a power-law truncation of the inner boundary as in Pavlyuchenkov, Maksimova & Akimkin (2022):

$$\Sigma(R) = \Sigma_0 \left(1 - e^{-\left(\frac{R}{R_0}\right)^p} \right) \left(\frac{R}{1 \text{ au}} \right)^{-1}, \quad (13)$$

where $\Sigma_0 = 200 \text{ g cm}^{-2}$ is the normalization of the surface density; $R_0 = 3 \text{ au}$ and $p = 8$ are the parameters of smoothing the density distribution near the inner boundary of the disk. The inner and outer boundaries of the disk are 1 and 20 au. The mass, temperature, and luminosity of the central star are $M = 1M_\odot$, $T_* = 6000 \text{ K}$, and $L = 5L_\odot$, respectively. At the outer boundary of the computational domain, we specify a background density of $10^{-19} \text{ g cm}^{-3}$, zero velocity components, and a background IR radiation temperature of 10 K.

3 APPROXIMATE MODELS OF A GAS AND DUST DISK

The aim of this work is to study the role of two-dimensional effects in the generation of thermal surface waves. For this, along with the basic two-dimensional model, we considered models in which the approximations that we used in the previously presented 1+1D model by Pavlyuchenkov, Maksimova & Akimkin (2022) are successively replaced with more rigorous ones. Along with full-valued 2D hydrodynamics (2D HD), we considered models in which the gas is in hydrostatic equilibrium in the θ direction (1D static). In addition to the 2D approximation in the transfer of IR radiation (2D RT), we also considered models in which IR radiation can only propagate in the θ direction (1D RT). Figure 3 shows the combinations of models we have considered, and below we briefly describe the implementation of the approximations used.

Note that the "1D static & 1D RT" combination is most similar in formulation to the model from our previous work (Pavlyuchenkov, Maksimova & Akimkin 2022). In this article, we consider the "1D static & 1D RT" model in order to reproduce the surface wave formation process obtained in Pavlyuchenkov, Maksimova & Akimkin (2022) on a Cartesian grid.

3.1 Hydrostatic Approximation

We calculate the disk structure within this approximation based on the solution of the following equation:

$$\frac{1}{\rho} \frac{d(\rho T)}{d\psi} = -\beta\psi, \quad (14)$$

where $\psi = \pi/2 - \theta$ is the angle measured from the equatorial plane of the disk, $\beta = \frac{GM}{R_\mu r_c}$, $R_\mu = \frac{k_B}{\mu m_a}$, k_B the Boltzmann constant, $\mu = 2.3$ is the average molecular weight, m_a is the atomic mass unit, and r_c is the radial distance to the cell center. Equation (14) can be derived from the equation for a vertically hydrostatic disk, assuming that the ratio z/r is small. However, we use Eq. (14) for all cells of the computational domain. When integrating Eq. (14) numerically, we assume that the temperatures in the cells are known (determined after calculating the radiative transfer). An additional condition for integrating Eq. (14) is the preservation of the mass of the entire θ -column of cells. Thus, in this approach, we allow the substance to be redistributed in the θ direction, adjusting to the current thermal structure. Of course, such a disk will not be hydrostatic in the physical sense, since Eq. (14) is approximate and incorrect as $z/r \sim 1$. However, it qualitatively correctly reflects the dependence of the disk height on the thermal structure and is easily solved on a spherical grid; therefore, it is convenient to use to study the disk instability.

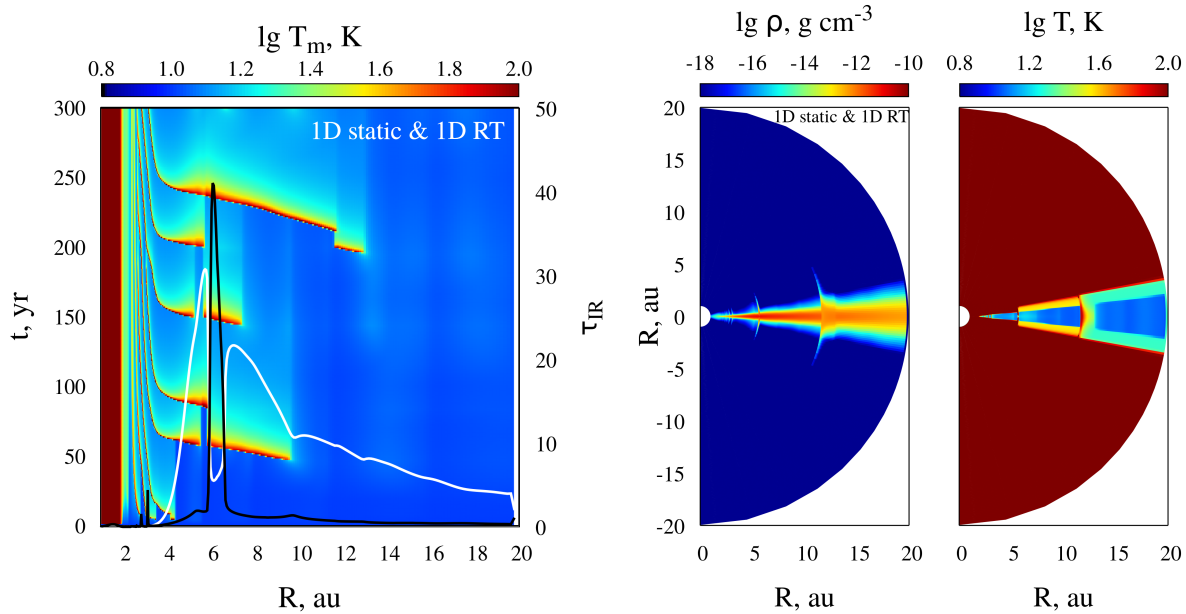


Figure 4. Calculation results for the “1D static & 1D RT model”: (left) evolution of equatorial temperature over the first 300 years, (white line) characteristic thermal time for the entire disk thickness, (black line) vertical optical thickness to thermal radiation, and (right) density and temperature distributions in the polar section of the disk at a time point of 200 years.

3.2 One-Dimensional Thermal Model

In this approximation, we assume that IR radiation propagates only in the θ direction, while the UV radiation of the star heats the disk only in the radial direction. Within the equations described in Section 2 and Appendix B, this approximation is realized by zeroing the fluxes $F_{r,ra}$ and $F_{r,rb}$ in expression (B3), after which the determination of the thermal structure is divided into a number of one-dimensional problems. The corresponding finite-difference equations are solved using the tridiagonal matrix algorithm. In this case, an important point is to impose appropriate boundary conditions: if we formally take all the cells with the same θ in the difference scheme obtained, then the radiation inside this array will be blocked, since the areas of the cell faces that are in contact with the polar axis are equal to zero ($S_{\theta a} = 0$ at $\theta = 0$ and $S_{\theta b} = 0$ at $\theta = \pi$). Therefore, we artificially set the radiation energy density in the polar cells equal to the interstellar background. Note that this approximation, like the model of hydrostatic equilibrium with respect to the angle θ , is, of course, quite rough and cannot be considered useful for practical application. We use it only as a tool for testing the approximations underlying the 1+1D analytical models of surface wave generation.

4 SIMULATION RESULTS

In this section, we describe the results of numerical simulation of surface waves, starting with models with the simplest interpretation of physical processes (hydrostatic and one-dimensional). Figure 4 (left) presents the results of calculating the evolution of the equatorial disk temperature in the first 300 years using the “1D static & 1D RT model”.

The distribution clearly shows perturbations originating within 15 au and propagating from outside to inside. The emergence period and propagation time of perturbations is ~ 50 years,

which is comparable to the characteristic thermal time $t_{th} = \frac{3}{8} \frac{c_V \Sigma^2 \kappa_R(T_m)}{\sigma_{SB} T_m^3}$, whose distribution is shown by the white line taken for the time point of 300 years. In this distribution, the waves propagating from outside to inside have discontinuities (see, e.g., the region in the vicinity of 6 au at a time point of 150 years). These discontinuities are associated with the formation of an inner hump on the disk surface, which begins to obscure the currently existing outer hump. After the inner hump reaches the inner boundary of the disk, the outer hump recovers and continues its propagation from the place where it stopped at the time of the eclipse (the eclipse time is less than the cooling time of the outer hump).

Figure 4 (left) also shows (by the black line) the distribution of the optical thickness $\tau_{IR} = \kappa_P \Sigma(R)$ in the vertical direction to the disk’s own thermal radiation at a time point of 300 years. A strong peak in the vicinity of 6 au is associated with an increase in temperature (and, accordingly, an increase in $\kappa_P(T)$) in this region due to the emerging thermal perturbation. The optical depth exceeds unity in the region of 4–10 au, which justifies the use of the Eddington approximation for calculating the diffusion of thermal radiation.

Figure 4 (right) shows two-dimensional density and temperature distributions in the polar section of the disk at a time point of 200 years. The distributions clearly show two arc-shaped perturbations in the vicinity of 5 and 12 au. This form of perturbations is associated with the assumption of the hydrostatic model that the matter is redistributed only in the θ direction. For each radial position in the disk, the temperature decreases from the atmosphere towards the equator, which is typical of a classical passive disk. The temperature in the region of the humps, which receive a greater share of stellar radiation, is increased. The temperature also increases over ~ 2 au behind the humps, which is related to the finite time of disk cooling due to its own IR radiation. This qualitative picture of disk evolution is similar to that presented in our previous work (Pavlyuchenkov, Maksimova & Akimkin 2022) for a

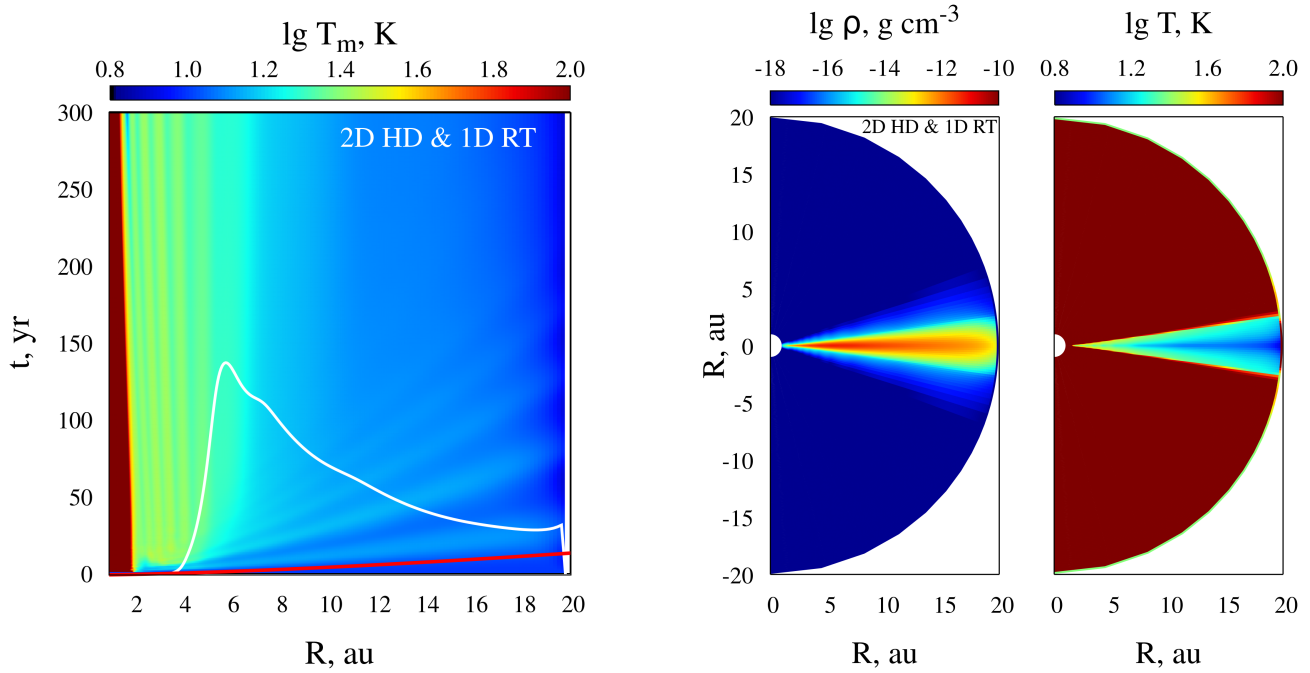


Figure 5. Calculation results for the "2D HD & 1D RT model": (left) equatorial temperature over the first 300 years, (white line) characteristic thermal time for the entire disk thickness, (red line) characteristic dynamic (Keplerian) time. The numerical scale for these times coincides with the scale for evolution time. (Right) Density and temperature distributions in the polar section of the disk at a time point of 200 years.

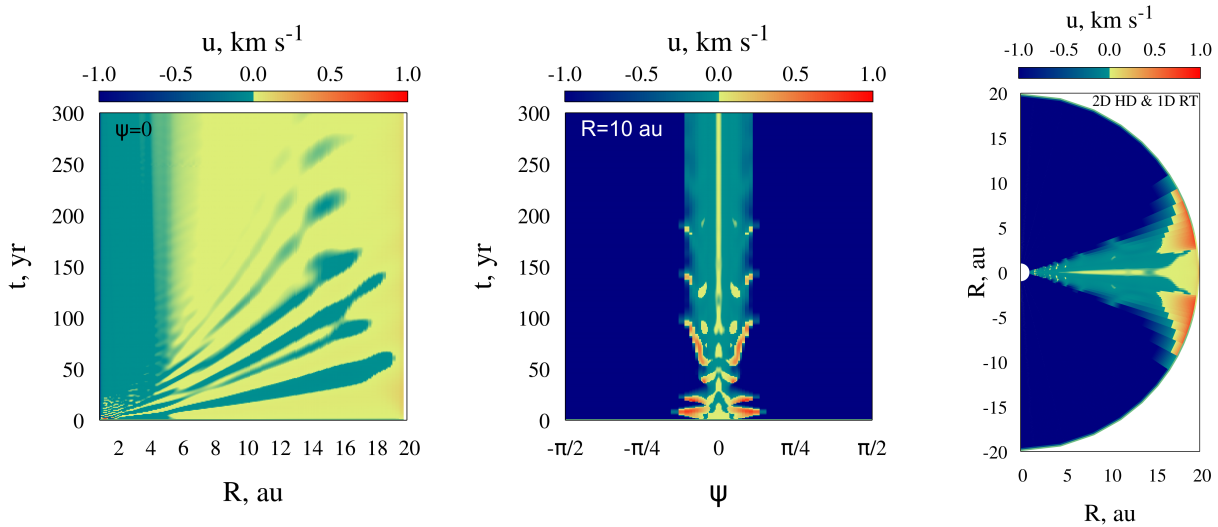


Figure 6. Calculation results for the "2D HD & 1D RT model": (left) evolution of the radial velocity distribution $u(r)$ in the equatorial plane of the disk; (center) evolution of the latitudinal distribution of the radial velocity $u(\psi)$, where ψ is the angle measured from the equator at a radius of 10 au; and (right) distribution of the radial velocity $u(r, \psi)$ in the polar section of the disk at a time point of 200 years.

disk model with similar initial parameters. Note that this model has a primarily methodological value, since the unrealistic (arc) shape of traveling perturbations, associated with a one-dimensional description of the disk structure and radiation transfer in the θ direction, does not allow using it in relation to any observations. At the same time, with the help of this model, we managed to reproduce the formation of thermal waves within the numerical code imple-

mented in a spherical coordinate system. This model serves as a starting point for our subsequent study of two-dimensional effects.

Figure 5 shows the results of calculating disk evolution within the "2D HD & 1D RT model". Considering the hydrodynamic effects completely changes the picture of disk evolution. In contrast to the "1D static & 1D RT model", in which waves periodically originate in the region of 6–15 au, perturbations in the "2D HD & 1D RT model" arise only at the initial times within 4 au and

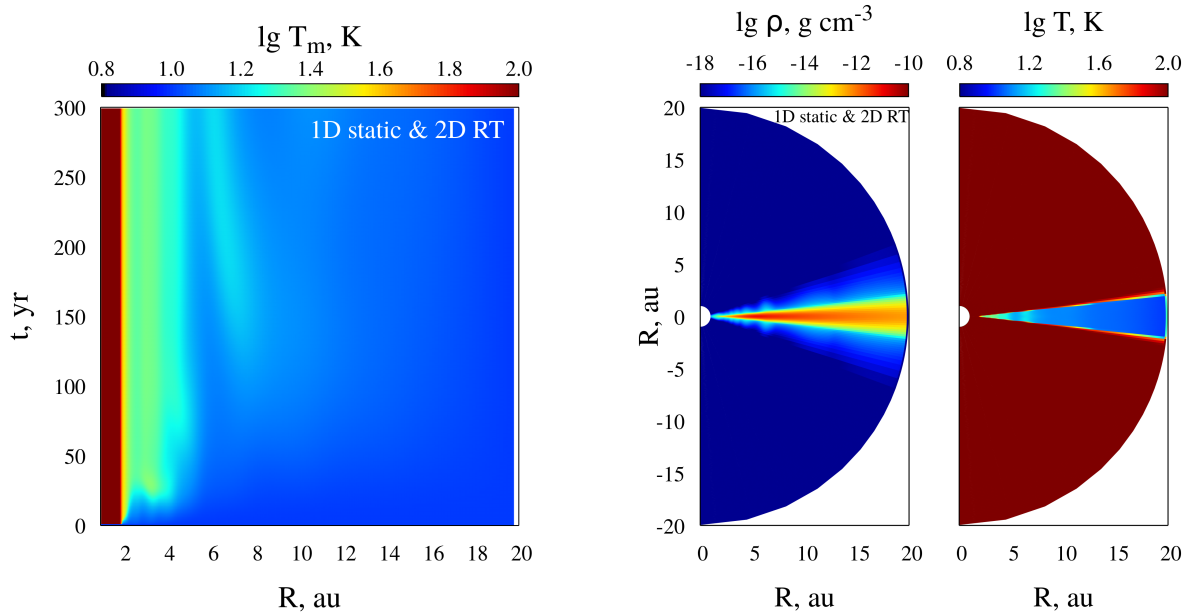


Figure 7. Calculation results for the "1D static & 2D RT model": (left) evolution of equatorial temperature over the first 300 years and (right) density and temperature distributions in the polar section of the disk at a time point of 200 years.

propagate outward. We believe that these perturbations are associated with a strong hydrodynamic nonequilibrium of the initial state of the disk. These waves decay with time and can be traced up to ~ 150 years. In the inner part of the disk ($r < 5$ au), a stationary annular structure is established. The density and temperature distributions in the polar section of the disk look smooth, except for weak annular perturbations in the inner regions of the disk. The thermal structure of the disk is standard for a passive disk: the disk atmosphere is warmer than the equatorial regions and there is a weak radial temperature gradient in the equatorial plane.

Figure 6 shows the evolution of the radial velocity u in the equatorial plane, as well as along the angular coordinate for cells at a radius of 10 au. These distributions illustrate the propagation and damping of hydrodynamic perturbations that arise at the initial moment of time. Perturbations of radial velocities $\Delta u \sim 0.2$ km/s are comparable to sound velocities $c_s = (k_B T_m / (\mu m_a))^{1/2} \approx 0.19$ km/s for $T_m = 10$ K. Note that velocity perturbations in the surface layers ($\psi \approx \pm 0.3$ radians) are higher than in the equatorial plane ($\psi = 0$). An interesting feature of these distributions is that, over time, a meridional circulation in the disk is established: in the surface parts of the disk, matter flows towards the star, while, in the equatorial region, matter flows outward. Strong velocity perturbations ~ 1 km/s at the outer boundary of the computational domain are associated with the boundary conditions imposed.

Thermal waves propagating from outside to inside do not arise in this model. We believe that the reason is that the emerging surface perturbations have time to smooth out dynamically before they have time to significantly warm the lower layers. Such smoothing is analogous to the process of relaxation of the initially nonequilibrium state described above. This assumption is supported by a comparison of the characteristic thermal time (duration of heating of the equatorial layers) and dynamic time $t_K = \sqrt{R^3 / (GM)}$, shown in the Fig. 5 (left) in white and red respectively. Indeed, in the region under consideration, the dynamic time is shorter than the thermal time. It should be noted that the condition of smallness of

dynamic time with respect to thermal time is used as a justification of using vertical hydrostatic equilibrium, which is the key approximation in the modern picture of thermal wave formation. However, the results of our simulation show that this condition leads to dynamic relaxation of perturbations in the radial direction. Based on this model, we conclude that hydrodynamic effects can suppress surface waves.

Figure 7 shows the results of calculating the disk evolution using the "1D static & 2D RT model". The character of disk evolution in this model differs significantly from the two models considered above. In this model, no periodic traveling waves arise, but several humps can be distinguished in the disk structure. The most noticeable hump is formed in the region of ~ 8 au at the time point of ~ 120 years and slowly moves inward, but, after 250 years, it becomes almost stationary. The temperature distribution in the polar section of the disk at a time point of 200 years is more uniform compared to the "2D HD & 1D RT model" and vertical temperature stratification is not so clearly manifested in it. We attribute this feature to obscuring the outer layers of the disk by internal quasistationary humps; in this case, the thermal structure is largely determined by the two-dimensional nature of the diffusion of IR radiation. The general conclusion from this model is that the two-dimensional transfer of IR radiation rather effectively blurs the thermal inhomogeneities of the disk, thereby suppressing (or many times slowing down compared to the "1D static & 1D RT model") the periodic formation and propagation of surface waves. At the same time, in this model, internal quasi-stationary perturbations are observed that intercept and process a significant fraction of the stellar radiation entering the disk.

The conclusions obtained within this model should be compared with the results of Okuzumi, Ueda & Turner (2022), where two-dimensional effects of radiative transfer are also considered in the hydrostatic approximation, but waves there are formed. The key difference between our models is that the thermal structure of the disk is described in Okuzumi, Ueda & Turner (2022) in the two-

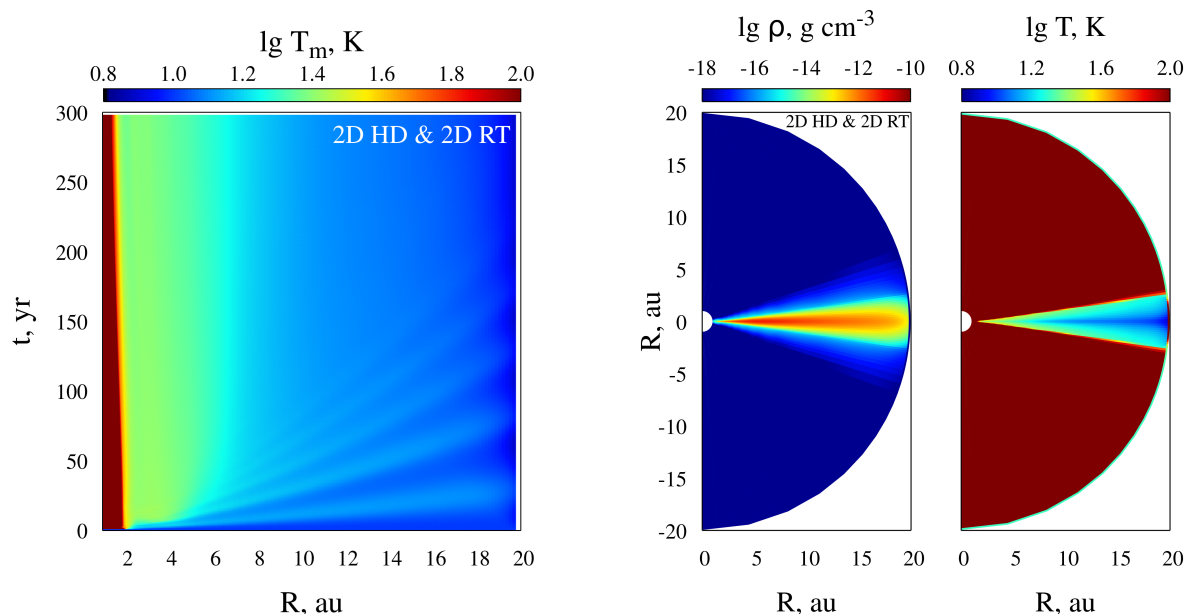


Figure 8. Calculation results for the "2D HD & 2D RT model": (left) evolution of equatorial temperature over the first 300 years and (right) density and temperature distributions in the polar section of the disk at a time point of 200 years.

zone approximation, while the characteristic height of the disk is determined by the equatorial temperature. In our model, the hydrostatic structure of the disk is built in accordance with the vertical temperature profile. In addition, Okuzumi, Ueda & Turner (2022) uses a different method for calculating the transfer of thermal radiation based on direct integration, while our approach uses the diffusion method. As a result, it can be assumed that, within our model, the relaxation of thermal inhomogeneities is more efficient, which does not lead to their growth.

Finally, Fig. 8 shows the results of calculating the disk evolution using the "2D HD & 2D RT model". The dynamics and structure of the disk within this model is close to that observed in the "2D HD & 1D RT model". The only significant difference between them is that, in the "2D HD & 2D RT model", the inner region of the disk ($r < 6$ au) has become homogeneous and is not divided into rings. The structure of the disk in the $(r\theta)$ plane corresponds to a passive disk with pronounced vertical thermal stratification. Based on the results of this model, a global conclusion can be drawn that the joint consideration of two-dimensional hydrodynamics and thermal radiative transfer suppresses the formation and propagation of surface thermal waves in gas and dust disks.

In connection with our results, it is worth noting the paper by Melon Fuksman & Klahr (2022), the preprint of which appeared at the stage of reviewing our work. Melon Fuksman & Klahr (2022) independently of us, using their numerical model, also came to the conclusion that thermal waves are suppressed if hydrodynamic effects and nonstationary character of heat transfer are considered.

5 CONCLUSIONS

This work is a logical continuation of the research presented in our article Pavlyuchenkov, Maksimova & Akimkin (2022). The main objective of this work was to study surface thermal waves in gas and dust disks with a more realistic description of the processes, considering two-dimensional hydrodynamic effects and

two-dimensional effects of thermal radiative transfer (in the $(r\theta)$ plane). To do this, we have developed a model of the evolution of an axisymmetric disk, destined to successively eliminate the approximations that underlie the modern theory of thermal surface waves. In this two-dimensional numerical code, we also implemented simplified approaches used in 1+1D models: the approximation of vertical hydrostatic equilibrium and vertical diffusion of IR radiation, and reproduced the formation of traveling surface waves from Pavlyuchenkov, Maksimova & Akimkin (2022). Then we showed that replacing the hydrostatic equilibrium approximation by hydrodynamic simulation leads to the disappearance of thermal surface waves. The same result is obtained when the one-dimensional approximation for calculating thermal radiation is replaced with two-dimensional simulation. Our results indicate that the jointly taking into account two-dimensional effects associated with hydrodynamics and thermal radiative transfer suppresses the development of thermal surface waves, which arise within the 1+1D approach.

The conclusion drawn here must be taken with some reservation due to the limitations of our model. The method we used for calculating the radiative transfer is based on the Eddington approximation, which assumes that the IR radiation field is isotropic. This approximation exaggerates the diffusion nature of radiation propagation in optically thin and transition regions and, therefore, leads to a more efficient smearing of inhomogeneities. It is necessary to verify the conclusions using more correct methods for calculating the radiative transfer, such as flux limited diffusion method (Levermore & Pomraning 1981) or the method of the variable Eddington tensor (Stone, Mihalas & Norman 1992). It was noted in Okuzumi, Ueda & Turner (2022) that the development of instability can also be suppressed by an insufficiently high spatial resolution of the numerical model. In our calculations, due to high computational costs, we were limited to a relatively sparse spatial grid ($N_r \times N_\theta = 360 \times 64$, but it is nonuniform). Therefore, further analysis on finer grids is necessary. It should be noted that our

conclusions cannot state that the development of instability is fundamentally impossible. Our results only show the absence of 2D surface waves under specific physical conditions, under which they are spontaneously formed in the 1+1D model. This problem should be investigated for a wide range of parameters of gas and dust disks, in particular, when the characteristic thermal and dynamic times are comparable.

APPENDIX A: FLUX VECTOR COMPONENTS FOR THE FINITE-DIFFERENCE EQUATION OF HYDRODYNAMICS

The components of the flux vectors entering into Eq. (4) for a finite-difference grid in spherical coordinates, taking into account the axial symmetry of the problem, have the following form:

$$\Delta F_1 = F_{1a} - F_{1b}$$

$$\Delta F_2 = F_{2a} - F_{2b}$$

$$\Delta F_3 = F_{3a} - F_{3b}$$

$$\Delta F_4 = F_{4a} - F_{4b}$$

$$\Delta F_5 = F_{5a} - F_{5b}$$

$$\Delta G_1 = G_{1a} - G_{1b}$$

$$\Delta G_2 = G_{2a} \cos \theta - G_{2b} \cos \theta + G_{3a} \sin \theta + G_{3b} \sin \theta$$

$$\Delta G_3 = -G_{2a} \sin \theta - G_{2b} \sin \theta + G_{3a} \cos \theta - G_{3b} \cos \theta$$

$$\Delta G_4 = G_{4a} - G_{4b}$$

$$\Delta G_5 = G_{5a} - G_{5b}$$

$$\Delta H_1 = 0$$

$$\Delta H_2 = H_{4a} \sin \varphi \sin \theta + H_{4b} \sin \varphi \sin \theta$$

$$\Delta H_3 = H_{4a} \sin \varphi \cos \theta + H_{4b} \sin \varphi \cos \theta$$

$$\Delta H_4 = -H_{2a} \sin \varphi \sin \theta - H_{2b} \sin \varphi \sin \theta \\ - H_{3a} \sin \varphi \cos \theta - H_{3b} \sin \varphi \cos \theta$$

$$\Delta H_5 = 0,$$

where

$$F_{1a} = (\tilde{\rho}\tilde{u})_{ra} S_{ra}$$

$$F_{1b} = (\tilde{\rho}\tilde{u})_{rb} S_{rb}$$

$$F_{2a} = (\tilde{\rho}\tilde{u}^2 + \tilde{P})_{ra} S_{ra}$$

$$F_{2b} = (\tilde{\rho}\tilde{u}^2 + \tilde{P})_{rb} S_{rb}$$

$$F_{3a} = (\tilde{\rho}\tilde{u}\tilde{v})_{ra} S_{ra}$$

$$F_{3b} = (\tilde{\rho}\tilde{u}\tilde{v})_{rb} S_{rb}$$

$$F_{4a} = (\tilde{\rho}\tilde{u}\tilde{w})_{ra} S_{ra}$$

$$F_{4b} = (\tilde{\rho}\tilde{u}\tilde{w})_{rb} S_{rb}$$

$$F_{5a} = (\tilde{E} + \tilde{P}\tilde{u})_{ra} S_{ra}$$

$$F_{5b} = (\tilde{E} + \tilde{P}\tilde{u})_{rb} S_{rb}$$

$$G_{1a} = (\tilde{\rho}\tilde{v})_{\theta a} S_{\theta a}$$

$$G_{1b} = (\tilde{\rho}\tilde{v})_{\theta b} S_{\theta b}$$

$$G_{2a} = (\tilde{\rho}\tilde{v}\tilde{u})_{ra} S_{\theta a}$$

$$G_{2b} = (\tilde{\rho}\tilde{v}\tilde{u})_{rb} S_{\theta b}$$

$$G_{3a} = (\tilde{\rho}\tilde{v}^2 + \tilde{P})_{\theta a} S_{\theta a}$$

$$G_{3b} = (\tilde{\rho}\tilde{v}^2 + \tilde{P})_{\theta b} S_{\theta b}$$

$$G_{4a} = (\tilde{\rho}\tilde{v}\tilde{w})_{\theta a} S_{\theta a}$$

$$G_{4b} = (\tilde{\rho}\tilde{v}\tilde{w})_{\theta b} S_{\theta b}$$

$$G_{5a} = (\tilde{E} + \tilde{P}\tilde{v})_{\theta a} S_{\theta a}$$

$$G_{5b} = (\tilde{E} + \tilde{P}\tilde{v})_{\theta b} S_{\theta b}$$

$$H_{2a} = (\tilde{\rho}\tilde{w}\tilde{u})_{\varphi a} S_{\varphi a}$$

$$H_{2b} = (\tilde{\rho}\tilde{w}\tilde{u})_{\varphi b} S_{\varphi b}$$

$$H_{3a} = (\tilde{\rho}\tilde{w}\tilde{v})_{\varphi a} S_{\varphi a}$$

$$H_{3b} = (\tilde{\rho}\tilde{w}\tilde{v})_{\varphi b} S_{\varphi b}$$

$$H_{4a} = (\tilde{\rho}\tilde{w}^2 + \tilde{P})_{\varphi a} S_{\varphi a}$$

$$H_{4b} = (\tilde{\rho}\tilde{w}^2 + \tilde{P})_{\varphi b} S_{\varphi b}$$

In the above expressions, the tilde denotes the quantities found from the solution of the problem of the decay of an arbitrary discontinuity for the corresponding cell's face, marked with a subscript; S_{ra} , S_{rb} , $S_{\theta a}$, $S_{\theta b}$, $S_{\varphi a}$, and $S_{\varphi b}$ are the areas of the cell's faces (see Fig. 2). Note that the trigonometric functions and the mixing of the flux components in the above expressions for the components of ΔG and ΔH are associated with the transformation of the local basis (and, accordingly, the coordinates of the velocity vectors) upon the transition between cells in θ and φ . At the same time, zero values for ΔH_1 and ΔH_5 are obtained taking into account the assumed axial symmetry of the problem.

APPENDIX B: METHOD FOR SOLVING THE SYSTEM OF THERMAL RADIATIVE TRANSFER EQUATIONS

The system of equations for the thermal evolution of the medium (10)–(11) is solved using Newton's iterations; for this, the equations are linearized using the approximation

$$T^4 \approx 4T_k^3 T - 3T_k^4,$$

where T_k is the temperature value at the previous (k -th) iteration, after which Eqs. (10)–(11) can be reduced to

$$T = \frac{b_d + \omega_p \Delta t E_r}{c_d + c_r} \quad (\text{B1})$$

$$\left[1 + \frac{c_d}{c_d + c_r} \omega_p \Delta t - \Delta t \hat{\Lambda} \right] E_r = g. \quad (\text{B2})$$

The coefficients c_d , ω_p , c_r , b_d , and g in these equations are calculated as follows:

$$c_d = \rho c_v$$

$$\omega_p = c_p \kappa_p$$

$$c_r = 4aT_k^3 \omega_p \Delta t$$

$$b_d = c_d T^n + \frac{3}{4} c_r T_k + \rho S \Delta t$$

$$g = E_r^n - \frac{3}{4} c_r T_k + \frac{c_r b_d}{c_d + c_r}.$$

We approximate the differential operator $\hat{\Lambda}$ in spherical coordinates in the following finite difference form:

$$\hat{\Lambda} E_r = \frac{1}{\Delta V} (S_{ra} F_{r,ra} - S_{rb} F_{r,rb} + S_{\theta a} F_{r,\theta a} - S_{\theta b} F_{r,\theta b}), \quad (\text{B3})$$

where ΔV is the cell volume and S_{ra} , S_{rb} , $S_{\theta a}$, and $S_{\theta b}$ are the current cell faces' areas (see Fig. 2). The fluxes through the cell's faces are found by the formulas

$$F_{r,ra} = -\frac{1}{\sigma_{ra}} \frac{E_r(i, j) - E_r(i-1, j)}{\Delta r_a}$$

$$F_{r,rb} = -\frac{1}{\sigma_{rb}} \frac{E_r(i+1, j) - E_r(i, j)}{\Delta r_b}$$

$$F_{r,\theta a} = -\frac{1}{\sigma_{\theta a}} \frac{E_r(i, j) - E_r(i, j-1)}{r_c \Delta \theta_a}$$

$$F_{r,\theta b} = -\frac{1}{\sigma_{\theta b}} \frac{E_r(i, j+1) - E_r(i, j)}{r_c \Delta \theta_b},$$

where $E_r(i, j)$ is the energy in the current cell with indices (i, j) , r_c is the radial coordinate of the center of the current cell, the values of $\sigma = 3\rho\kappa_R/c$ are calculated based on the gas density and medium temperature for the corresponding faces by interpolating the central values, and Δr and $r\Delta\theta$ are the distances from the center of the current cell to the centers of adjacent cells for the corresponding faces

(see Fig. 2). With this, Eq. (B2) can be rewritten in the following operator form:

$$\hat{\Omega}E_r = \mathbf{g}, \quad (\text{B4})$$

where $\hat{\Omega} = \left(1 + \frac{c_d}{c_d + c_r} \omega_p \Delta t\right) \hat{I} - \Delta t \hat{\Lambda}$, and \hat{I} is the unit tensor.

Equation (B4) is a compact representation of a system of linear algebraic equations with a sparse five-diagonal matrix. We solve this system of equations using the GMRES method (Saad & Schultz 1986) or the alternating direction implicit (ADI) method (Samarskii & Nikolaev 1978), depending on the complexity of the problem. Our numerical experiments with this model show that the GMRES method has good stability, but is several times slower than the ADI method. For the ADI method, the choice of iterative parameters is important, which we find based on the closeness of the results to the solution of the system by the GMRES method.

ACKNOWLEDGMENTS

We are grateful to the referee for valuable comments and suggestions for improving the article.

FUNDING

This work was supported by the Russian Foundation for Basic Research (project no. 20-32-90103). V. V. Akimkin acknowledges the support by the Theoretical Physics and Mathematics Advancement Foundation “BASIS” (grant no.20-1-2-20-1).

CONFLICT OF INTEREST

The authors declare that they have no conflicts of interest.

REFERENCES

- Abakumov M. V., 2014, *Prikladnaya matematika i informatika*, 45, 63
- Balbus S. A., Hawley J. F., 1991, *ApJ*, 376, 214
- Dullemond C. P., 2000, *A&A*, 361, L17
- Klahr H., Hubbard A., 2014, *ApJ*, 788, 21
- Kulikovskiy A. G., Pogorelov N. V., Semenov A. Y., 2012, *Matematicheskie voprosy chislennogo resheniya giperbolicheskikh system uravnenii*. Fizmatlit, Moskva
- Lesur G. R. J., Latter H., 2016, *MNRAS*, 462, 4549
- Levermore C. D., Pomraning G. C., 1981, *ApJ*, 248, 321
- Melon Fuksman J. D., Klahr H., 2022, *ApJ*, 936, 16
- Nelson R. P., Gressel O., Umurhan O. M., 2013, *MNRAS*, 435, 2610
- Okuzumi S., Ueda T., Turner N. J., 2022, arXiv e-prints, arXiv:2201.09241
- Pavlyuchenkov Y. N., Maksimova L. A., Akimkin V. V., 2022, *Astronomy Reports*, 66, 321
- Pavlyuchenkov Y. N., Tutukov A. V., Maksimova L. A., Vorobyov E. I., 2020, *Astronomy Reports*, 64, 1
- Saad Y., Schultz M. H., 1986, *SIAM Journal on Scientific and Statistical Computing*, 7, 856
- Samarskii A. A., Nikolaev E. S., 1978, *Metody resheniya setochnykh uravnenii*. Nauka, Moskva

- Semenov D., Henning T., Helling C., Ilgner M., Sedlmayr E., 2003, *Astron. and Astrophys.*, 410, 611
- Stone J. M., Mihalas D., Norman M. L., 1992, *Astrophys. J. Supp.*, 80, 819
- Ueda T., Flock M., Birnstiel T., 2021, *Astrophys. J. Lett.*, 914, L38
- Velikhov E. P., 1959, *Sov. Phys. JETP*, 36, 1398
- Vorobyov E. I., Pavlyuchenkov Y. N., 2017, *Astron. and Astrophys.*, 606, A5
- Watanabe S.-i., Lin D. N. C., 2008, *ApJ*, 672, 1183
- Wu Y., Lithwick Y., 2021, *ApJ*, 923, 123
- Youdin A. N., Goodman J., 2005, *ApJ*, 620, 459
- Zhuravlev V. V., 2022, *MNRAS*, 512, 2636